Chapter 4 Results and discussion

In this chapter, the morphology and optical properties of InN dots were studied by the atomic force microscopy (AFM) and temperature-dependent PL spectra.

4-1 Morphology study of InN dots

Four 5μm×5μm AFM top-view images of uncapped InN dots are shown in Fig. 4-1 (a) to (d). The respective substrate temperatures in Fig.4-1(a), (b) and (c) were 600, 625 and 650 ℃. It shows that the size of InN dots increases and the density decreases with increasing the substrate temperature. It also demonstrates the possibility of artificial size and density control by the substrate temperature. The respective histograms of number of dots versus dot height, (a) and (b), and versus dot width (c) and (d), for samples grown at 625 and 650 ℃ were shown in Fig 4-2. The average height is 18, 28±2 and 32±4 nm, the average width is 180, 216±18, and 253±18 nm, and the dot density is 8.4×10^{9}, 1.6×10^{9} and 8.9×10^{8} cm^{-2} for the growth temperature 600 ℃, 625℃ and 650 ℃, respectively. The average lateral width is far larger than the height and the aspect ratio (height/width) ranges from 1/10 to 1/13. Compared Fig. 4-1 (b) with Fig. 4-1 (d), the artificial size and density control also can be achieved by tuning TMIn deposition times. In Fig.4-1 (b) and (d), InN dots were grown at the same temperature (625 ℃), except TMIn deposition times decreases from 20 s/c to 10 s/c. The dot height/width decreases from 28 nm/210 nm to 24 nm/177 nm. One has to note that, in these InN dots, the spatial confinement of electrons and/or

holes should occur in the grown direction rather than in the lateral direction of a size of about 100 to 200 nm.

In Fig. 4-3, the morphology of a single InN dots was investigated. As shown in Fig. 4-3(a), the shape of most dots is hexagonal, which is similar to reports of other groups [7] [8]. However, there are a few dots which don't have nice hexagonal shape as shown in Fig. 4-3 (b). Some dots are formed by the stack of two dots as shown in Fig. 4-3 (c).

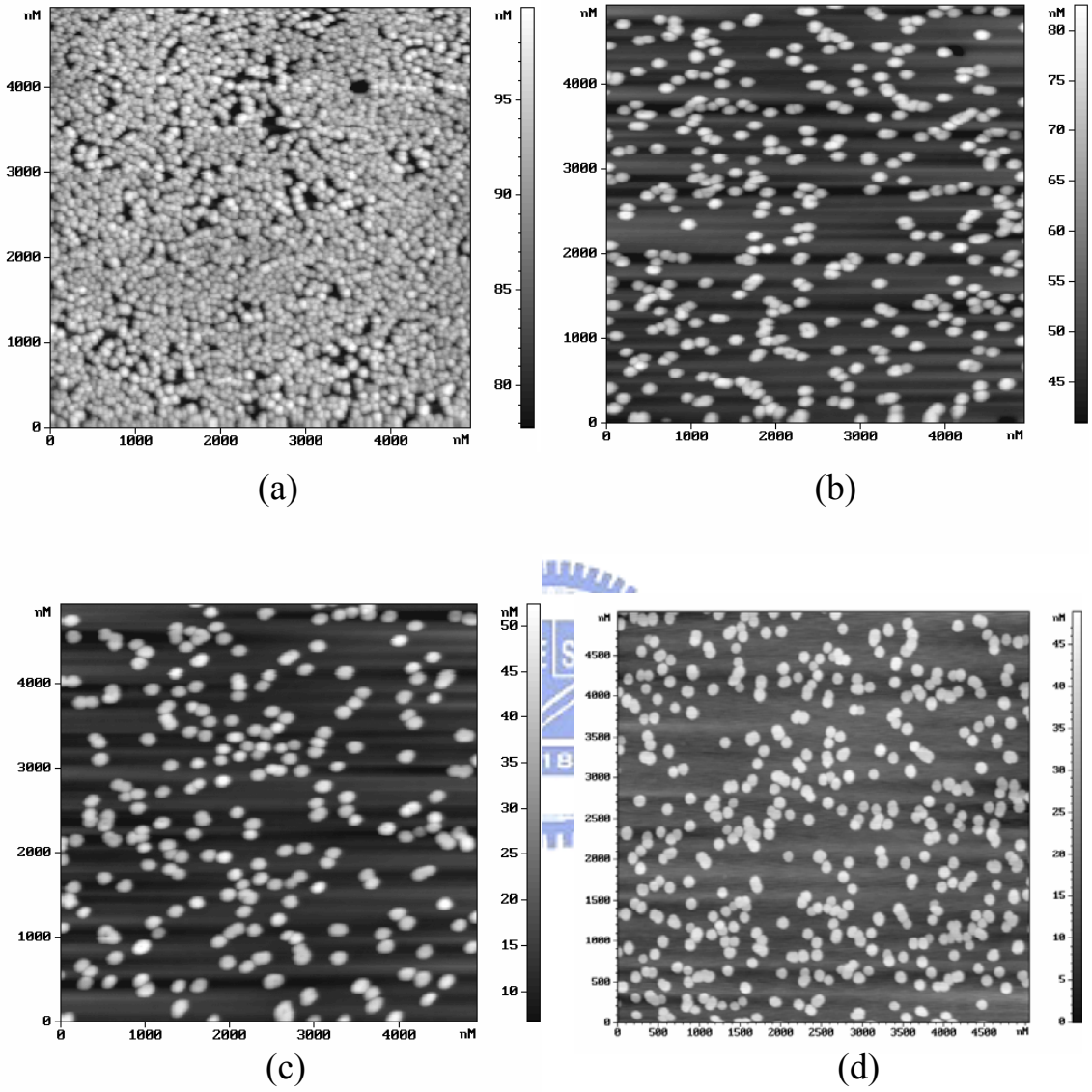

Fig. 4-1. Top-view AFM images of InN dots: (a) grown at 600 ℃, TMIn=20s/c and H/W~18nm/180nm, (b) grown at 625 ℃, TMIn=20s/c and H/W~28nm/216nm, (c) grown at 650 ℃, TMIn=20s/c and H/W~32nm/253nm and (d) grown at 625 ℃, TMIn=10s/c and H/W~24nm/177nm.

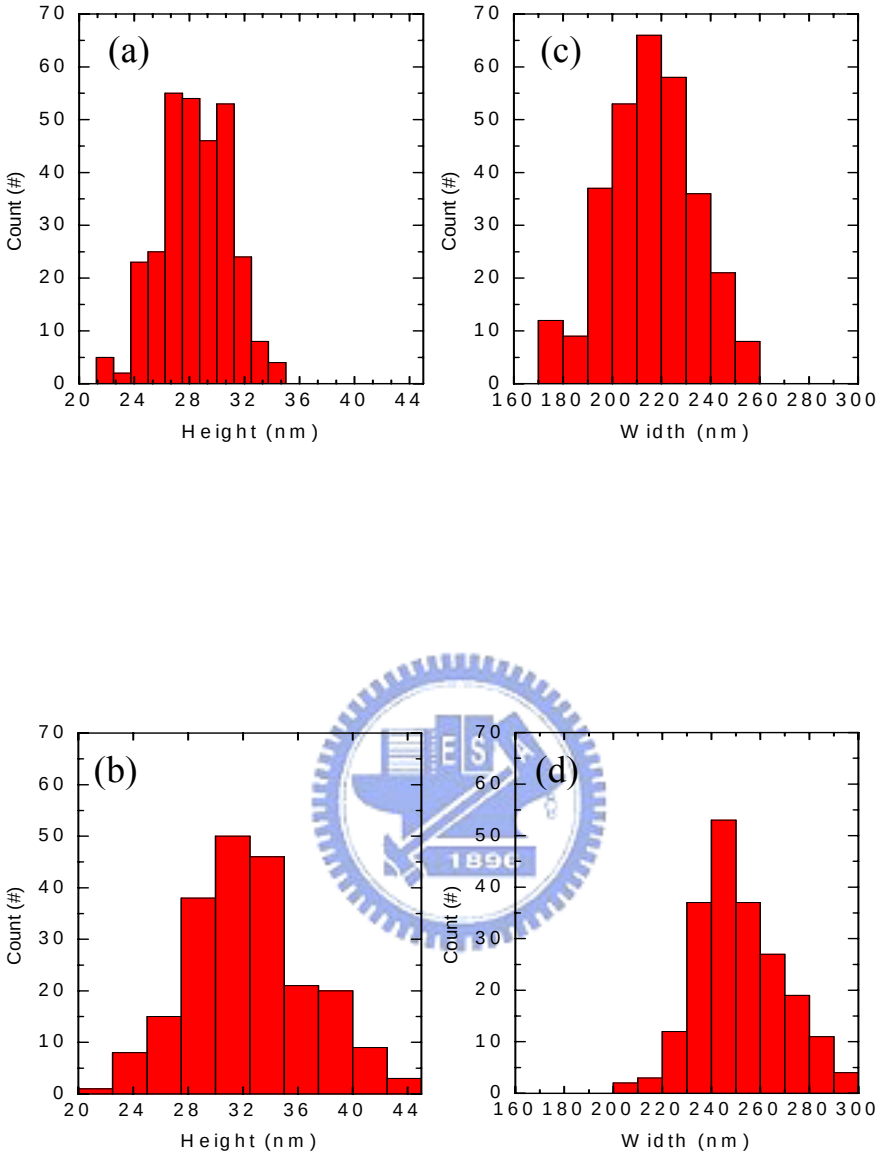

Fig. 4-2. Histograms of number of dots versus dot height, (a) and (b), and versus dot width, (c) and (d), for InN dots grown at substrate temperatures of 625 and 650 ℃, respectively. (a) H=28±2 nm, (b) H=32±4 nm, (c) W=216±18 nm, (d) W=253±18nm.

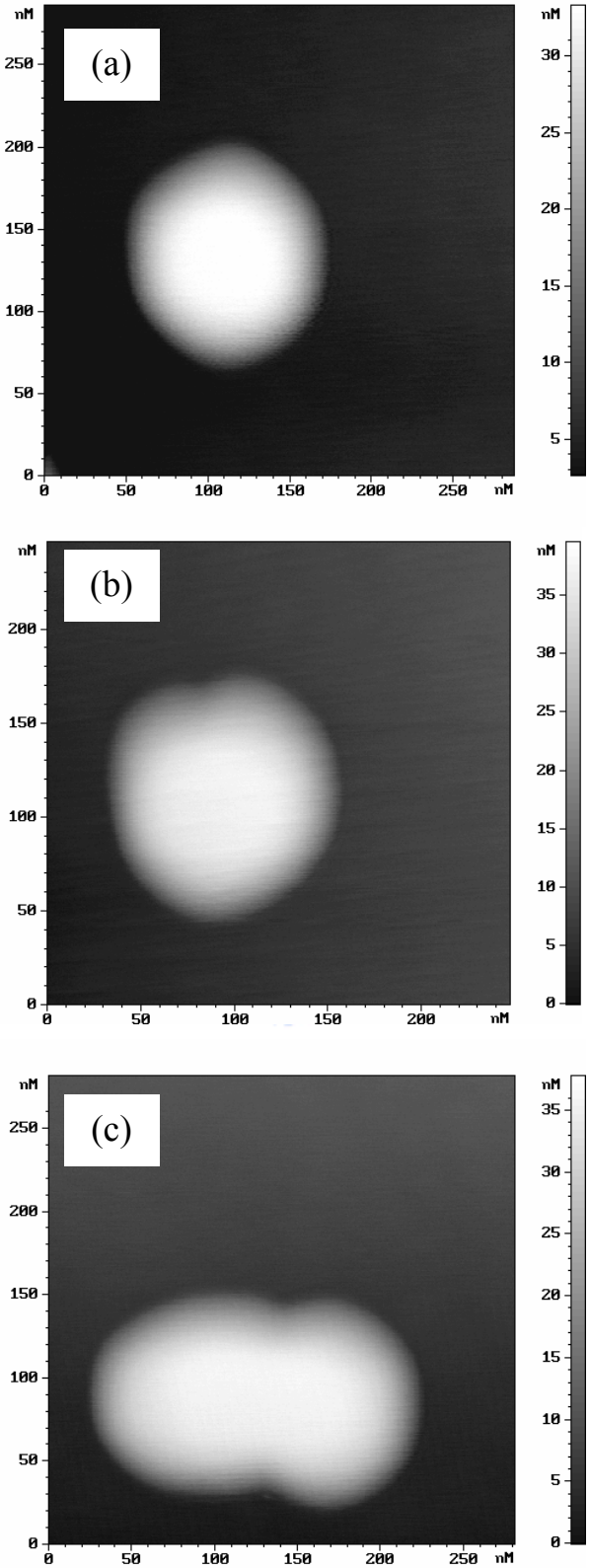

Fig. 4-3. Plane-view AFM images of a single InN dot.

4-2 PL spectra of InN epilayers and dots at low temperature

4-2-1 PL spectra of InN epilayers

Fig. 4-4 shows PL spectra of InN films with different carrier concentrations at 17 K. Peak energies of our InN films are larger than the reported band gap energy of 0.69 eV [9]. Due to the small effective mass of InN, the Fermi surface of the conduction band has shown a strong dependence on the carrier concentration. Thus, the shift of the PL peak position to higher energy was attributed to the Burstein-Moss effect [3] [6]. Moreover, the increase in full width at half maximum (FWHM) of PL spectra with increasing the electron concentration was observed. Table II summarizes the dependence of the E_{PL} and FWHM on the carrier concentration.

PL spectra of the InN epilayer are reported to be composed of two parts (I_{sh}, I_{da}) [9]. The dominant PL emission (I_{sh}) is the transition of degenerate electrons to shallow acceptors with a binding energy (E_{sh}) of 5-10 meV. The lower-energy shoulder of the PL emission (I_{da}) is attributed to the recombination of degenerate electrons with holes trapped by deep acceptors with a binding energy (E_{da}) of 50-55 meV [9]. And the schematic band diagram is shown in Fig. 4-5. According to the above discussion, we attribute the dominant PL emission of our epilayer with a carrier concentration of 7.9×10^{18} cm^{-3} at 0.764 eV is I_{sh}, and the lower-energy shoulder at 0.723 eV is I_{da}. However, so far, there is no report to identify the source and the type of shallow and deep acceptors.

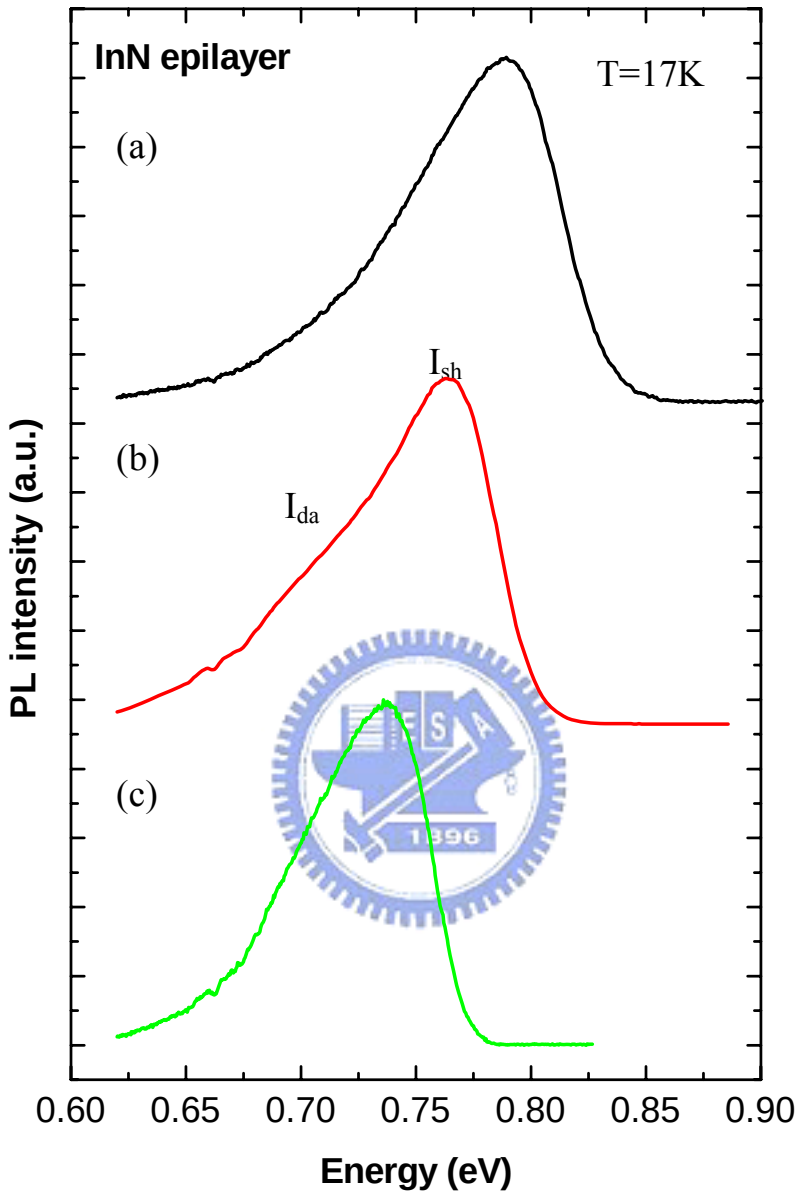

Fig. 4-4. Normalized PL spectra of InN epilayers with (a) $n=1.3\times10^{19}\,cm^{-3}$, (b) $n=7.9\times10^{18}\,cm^{-3}$ and (c) $n=6.4\times10^{18}\,cm^{-3}$

Table II. PL peak energies and FWHM of InN epilayers with different carrier concentrations at 17K.

Carrier concentration (cm^{-3})	E_{PL}(eV)	FWHM (meV)
(a) 1.3×10^{19}	0.784	90
(b) 7.9×10^{18}	0.764	82
(c) 6.4×10^{18}	0.739	73

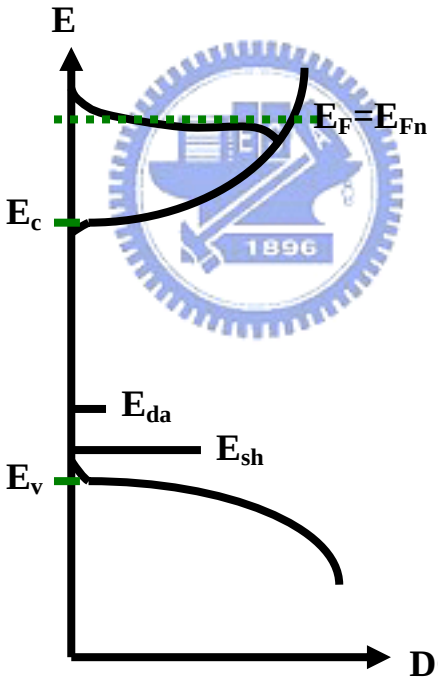

Fig. 4-5. Schematic diagram of the density of states, shallow and deep acceptor states, and the quasi-Fermi level with degenerate electrons in the conduction band.

4-2-2 Size-dependent PL spectra of InN dots

Fig. 4-6 (a) and (b) show PL spectra with various dot sizes controlled by tuning deposition times, and Fig. 4-6 (c) is the PL spectrum of the InN epilayer with the same growth temperature for reference. Fig. 4-6 reveals that the deep acceptor emission of dots is suppressed due to the improved crystal quality of self-assembled InN dots.

In Fig. 4-6 (b), the peak energy of the 28 nm InN dot shifts toward higher energy due to the size effect in the growth direction (height). Since diameters of InN dots are larger, the lateral confinement could be neglected. Estimated from the Hall measurement of the InN epilayer, the numbers of electrons may exceed 10000 in an InN dot. As a result, the energy blue-shift due to Burstein-Moss effect should not be excluded in these InN dot samples. In Fig. 4-6 (a), further decreasing the size to 24 nm/177 nm, the large blue-shift energy due to quantum confinement is observed. In addition, FWHM becomes broader than that of the 28 nm-dot and the epilayer due to significant size fluctuation of InN dots.

Fig. 4-7 shows PL spectra with various dot sizes grown with different substrate temperatures. The energy blue-shift for 18 nm/180 nm, 28 nm/216 nm and 32 nm/253 nm InN dots are 33, 20 and 6 meV, respectively. And these dots have better emission efficiency than dots whose sizes are controlled by tuning TMIn deposition times. In next section, we will focus on these dots to study the temperature dependent emission behavior of InN dots.

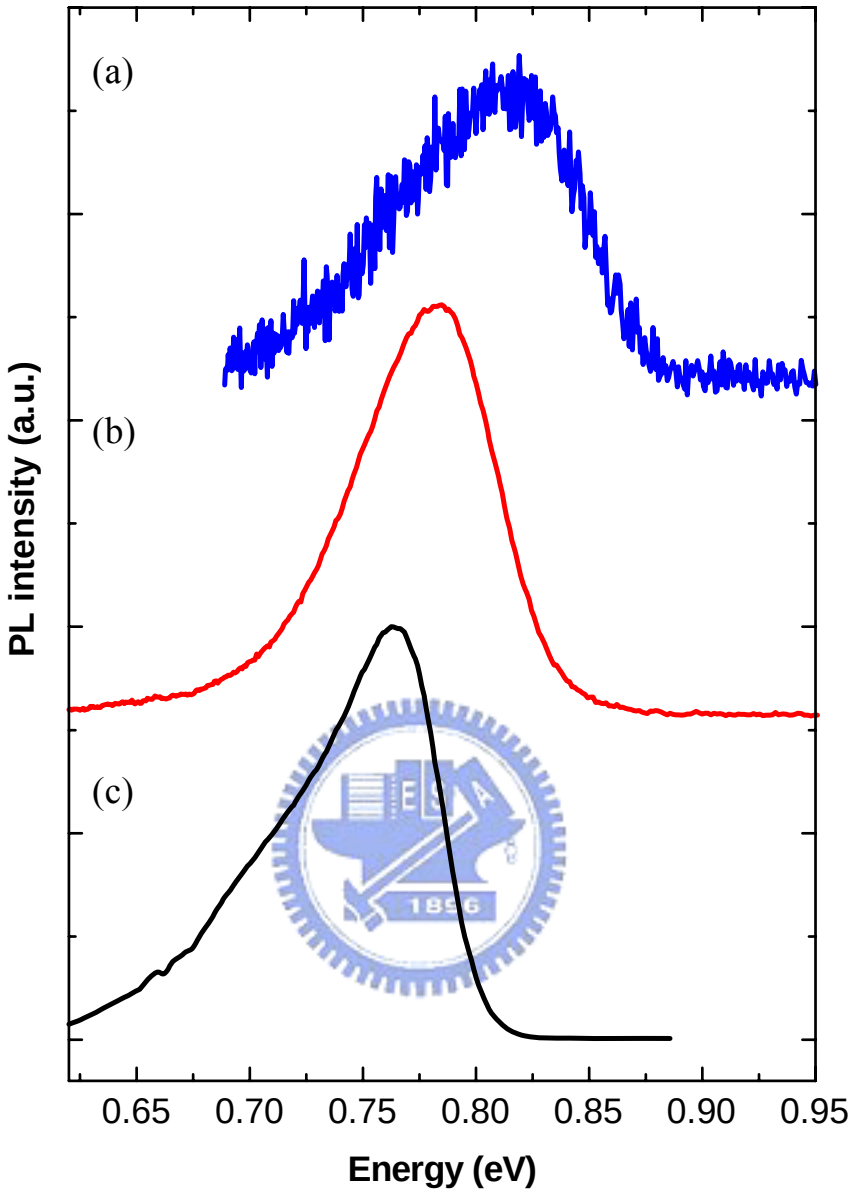

Fig. 4-6. Normalized PL spectra at 17K of (a) InN 24 nm-dots with E_{PL}=0.814 eV, (b) InN 28 nm-dots with E_{PL}=0.784 eV and (c) InN epilayer with E_{PL}=0.764 eV.

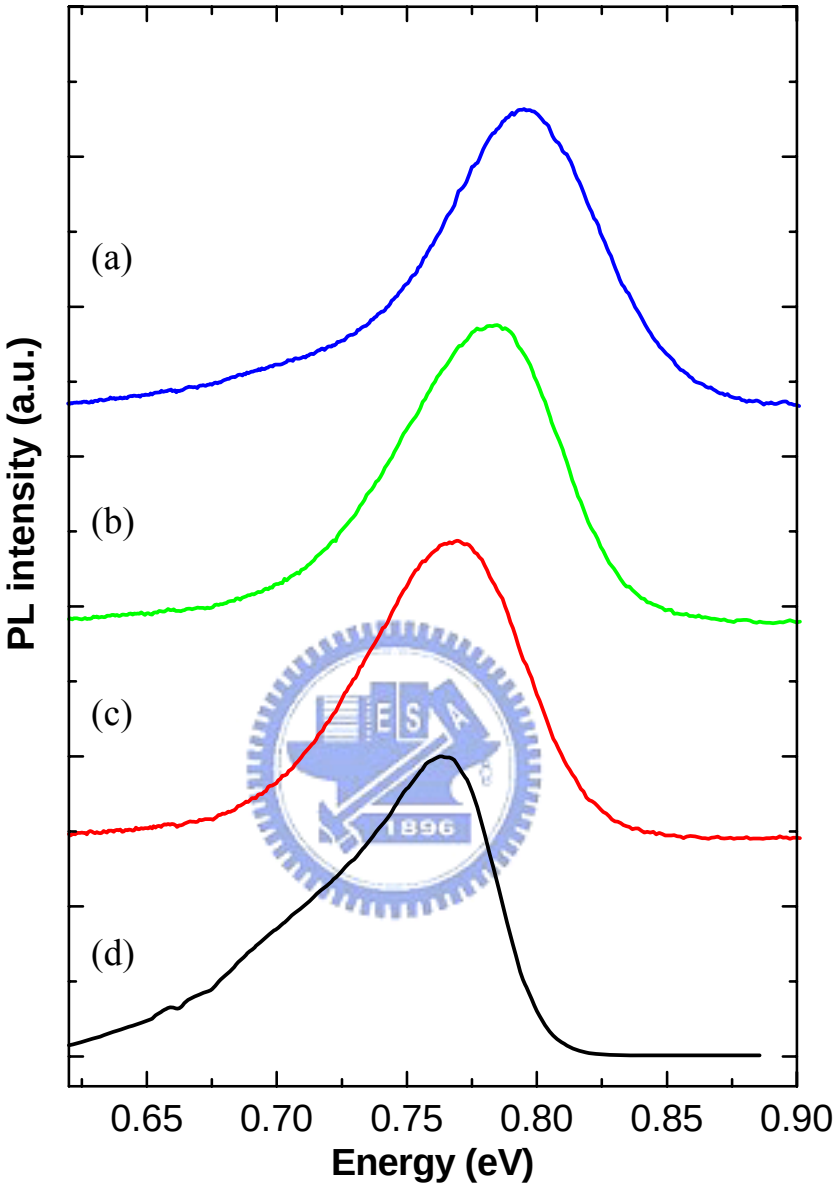

Fig. 4-7. Normalized PL spectra at 17K of (a) InN 18 nm-dots with E_{PL}=0.796 eV, (b) InN 28 nm-dots with E_{PL}=0.784 eV, (c) InN 32 nm-dots with E_{PL}=0.769 eV and (d) InN epilayer with E_{PL}=0.764 eV.

4-3 Temperature-dependent PL of the InN epilayer and dots

4-3-1 Temperature-dependent PL line shape and peak energy

Respective temperature-dependent PL spectra of the InN epilayer with carrier concentration of 7.9×10^{18} cm^{-3} and dots with height of 18 nm, 28 nm and 32 nm in the temperature ranging from 17 K to 300 K are shown in Fig. 4-8, 4-9, 4-10 and 4-11. Fig. 4-12 shows PL spectra of the InN epilayer and dots at temperatures 17 K (dashed line) and 300 K (solid line). The FWHM of the epilayer broadens and the PL peak energy shifts to lower energy with increasing temperature. The change in the PL line shape of the InN epilayer with increasing temperature could be due to the thermal redistribution of carriers [3].

However, in the case of InN dots, no significant line width broadening and no strong energy shift with increasing temperature was observed. Moreover, a high-energy shoulder (I_H) appears at higher temperatures. This high-energy PL shoulder (I_H) can be observed more clearly as the dot size increases. I_H appears at temperature above 150 K and 190 K for the 28 nm-dot and the 32 nm-dot, respectively. The Gaussian function was used to fit the PL line shape and obtain the peak energy shown in Fig. 4-13. Their respective energies of I_H at room temperature are 0.889 eV and 0.871 eV. The energy separations between the energy positions of I_{sh} and I_H are 111 meV and 109 meV for the 28 nm-dot and the 32 nm-dot, respectively. I_H peak of the 18 nm-dot is not clearly observed in temperature dependent PL spectra. It could be the intersubband transition ($\Gamma_1^v \rightarrow \Gamma_6^v$) with an energy separation of 0.093 eV [13]. However, the origin of I_H is not clear.

In Fig. 4-14, the PL peak energy (E_{PL}) of the InN epilayer and dots as a function of temperature is shown. PL peak energies of InN dots do not strongly

depend on temperature. As the temperature was increased from 17 K to 300 K, the energy of PL peak, E_{PL}, of the InN epilayer exhibits energy red-shift of about 54 meV. The red-shift energy follows the Varshni's prediction [10] which relates the temperature-induced shrinkage of the band gap to the thermal expansion of lattice structure and the electron-phonon interaction. On the other hand, PL peak energies red-shift with increasing temperature for 32 nm- and 28 nm-dots are only 6-7 meV. Furthermore, an energy blue-shift of 8 meV is observed in the 18 nm-dot as temperature was raised from 17 K to 300 K.

In degenerate semiconductors, a convolution between thermally distributed electrons and the holes localized near acceptors is needed to analyze PL spectra, so that the PL peak position can not be used to describe the energy position of the true band gap [10]. The reasons for no energy red-shift and/or energy blue-shift of PL emission with increasing temperature in InN dot samples could be similar to those reports of InN epilayers [9] [11] [12]. The shift of the PL peak energy in InN epilayers with increasing temperature have been observed and attributed to an increase in kinetic energies of carriers [9] or temperature-induced pushing up of non-equilibrium holes located in valence-band tails [11]. Moreover, there are still other reasons which could affect the shift of the PL peak energy such as an increase of the quasi-Fermi level due to non-equilibrium photo-generated carriers inject from the barrier or the difference of the polarization-induced electric field at low and room temperature. The polarization including the spontaneous and piezoelectric polarization in III-nitride heterostructures should be taken into account and the magnitude of the polarization-induced electric field was calculated by using the parameters which refer to the reports [14] [15] [16]. The magnitude of the field at low temperature is larger than that at room temperature for InN samples, so the

polarization-induced red-shift energy at low temperature is larger and that results in the blue-shift energy of the PL peak with increasing temperature. For the above reasons, the shift of the PL peak energy with increasing temperature could vary from sample to sample.

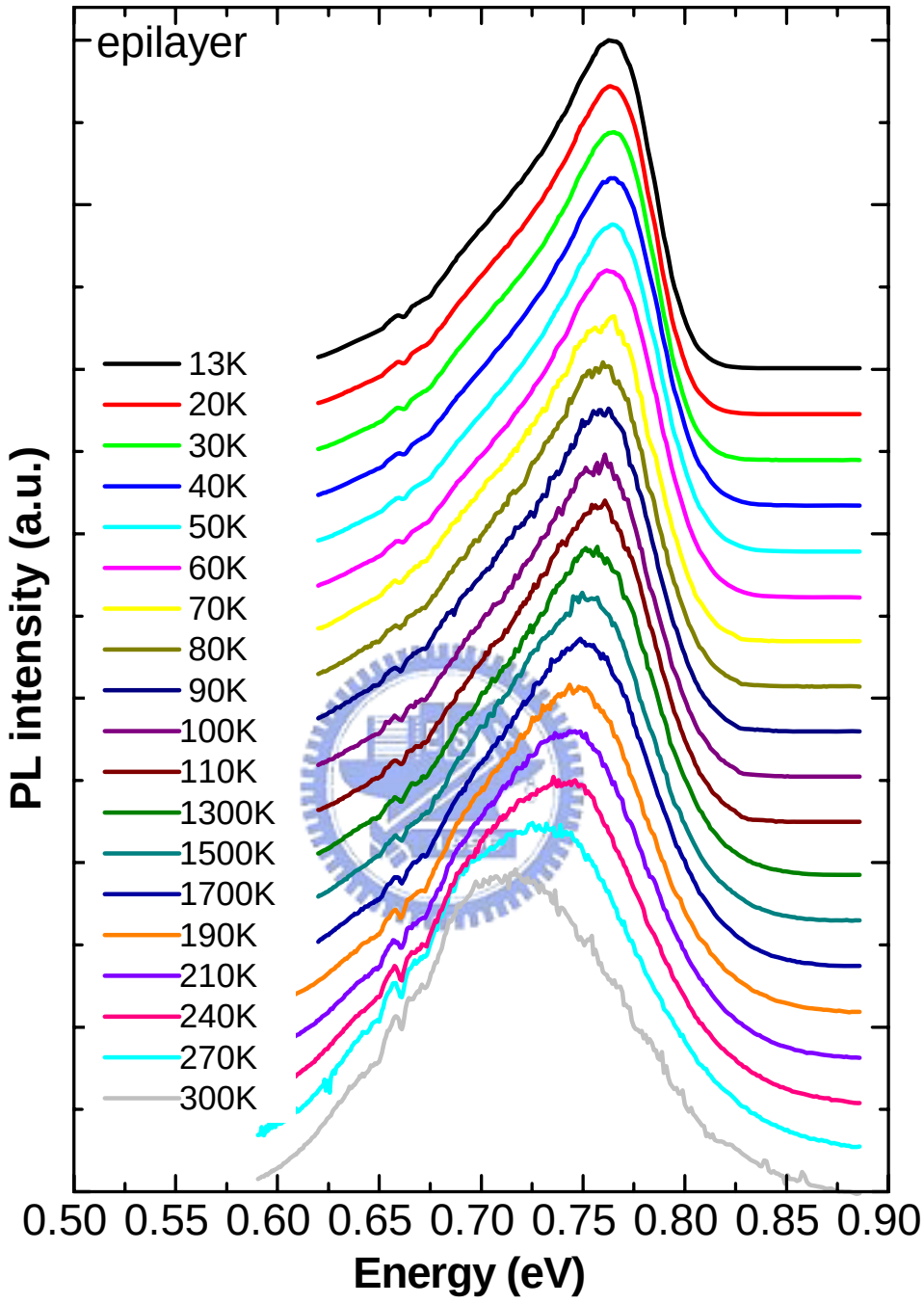

Fig. 4-8. PL spectra as a function of temperature for the InN epilayer with carrier concentration of 7.9×10^{18} cm^{-3}.

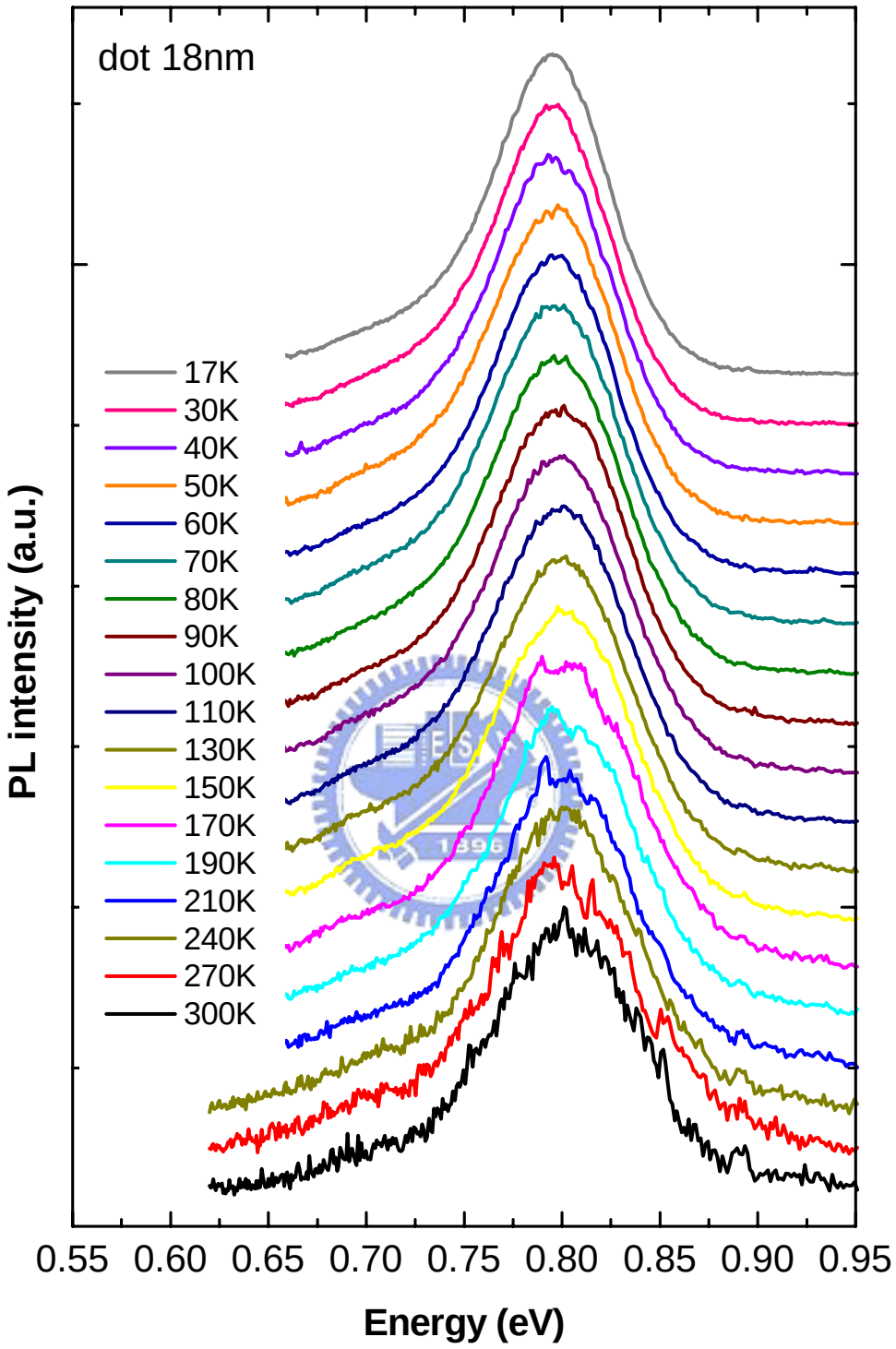

Fig. 4-9. PL spectra as a function of temperature for the InN dot of 18 nm in height.

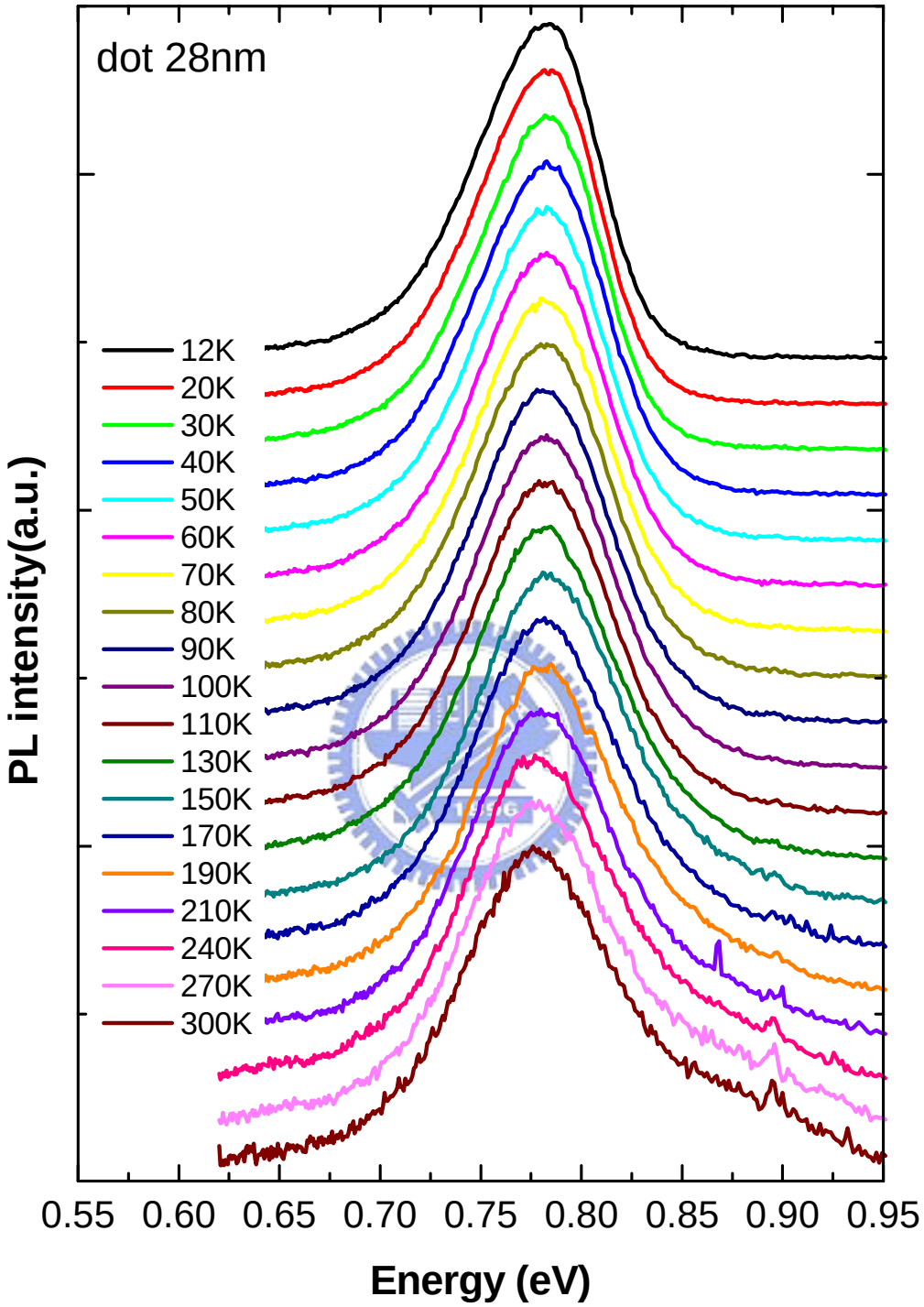

Fig. 4-10. PL spectra as a function of temperature for the InN dot of 28 nm in height.

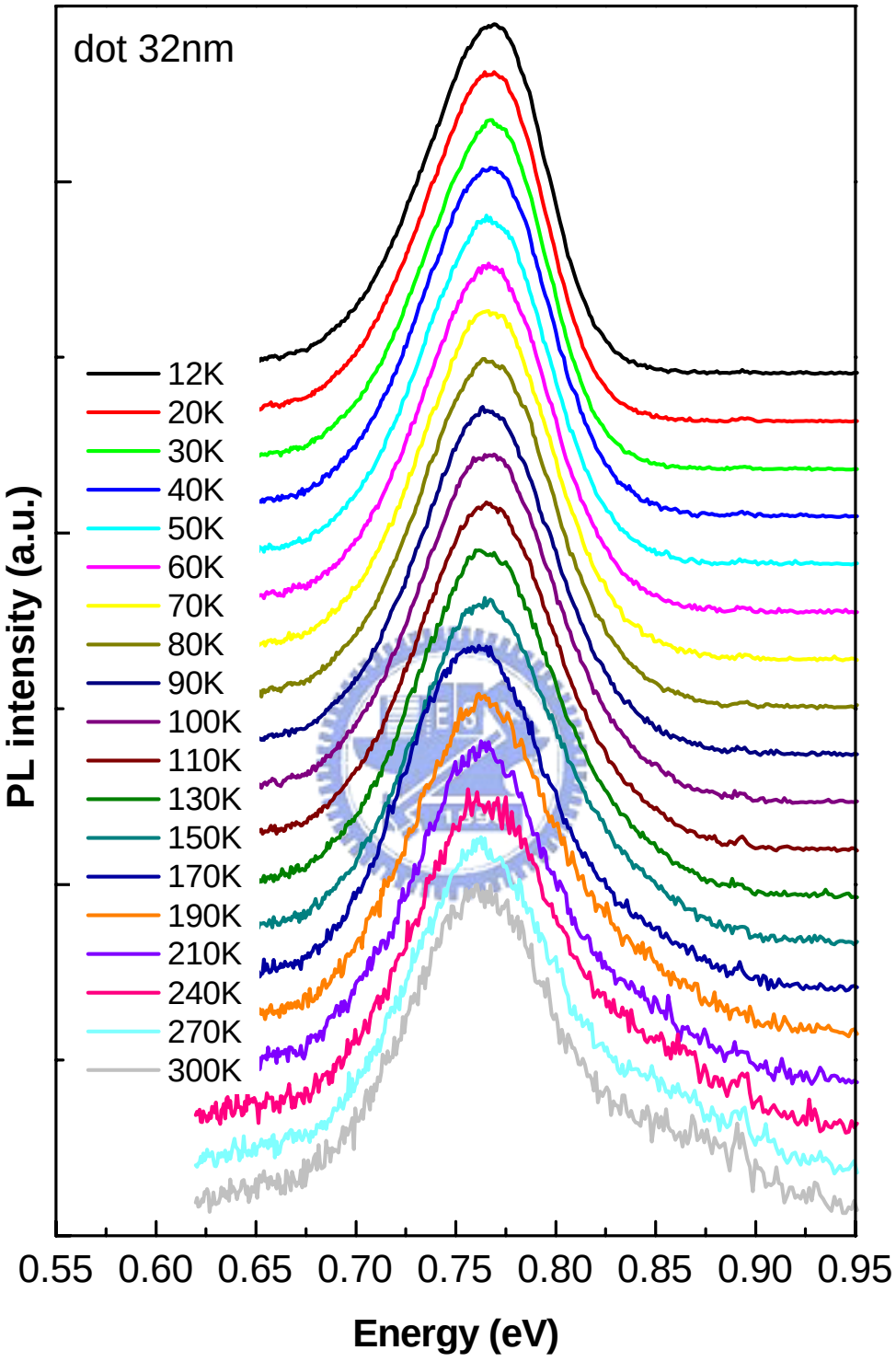

Fig. 4-11. PL spectra as a function of temperature for the InN dot of 32 nm in height.

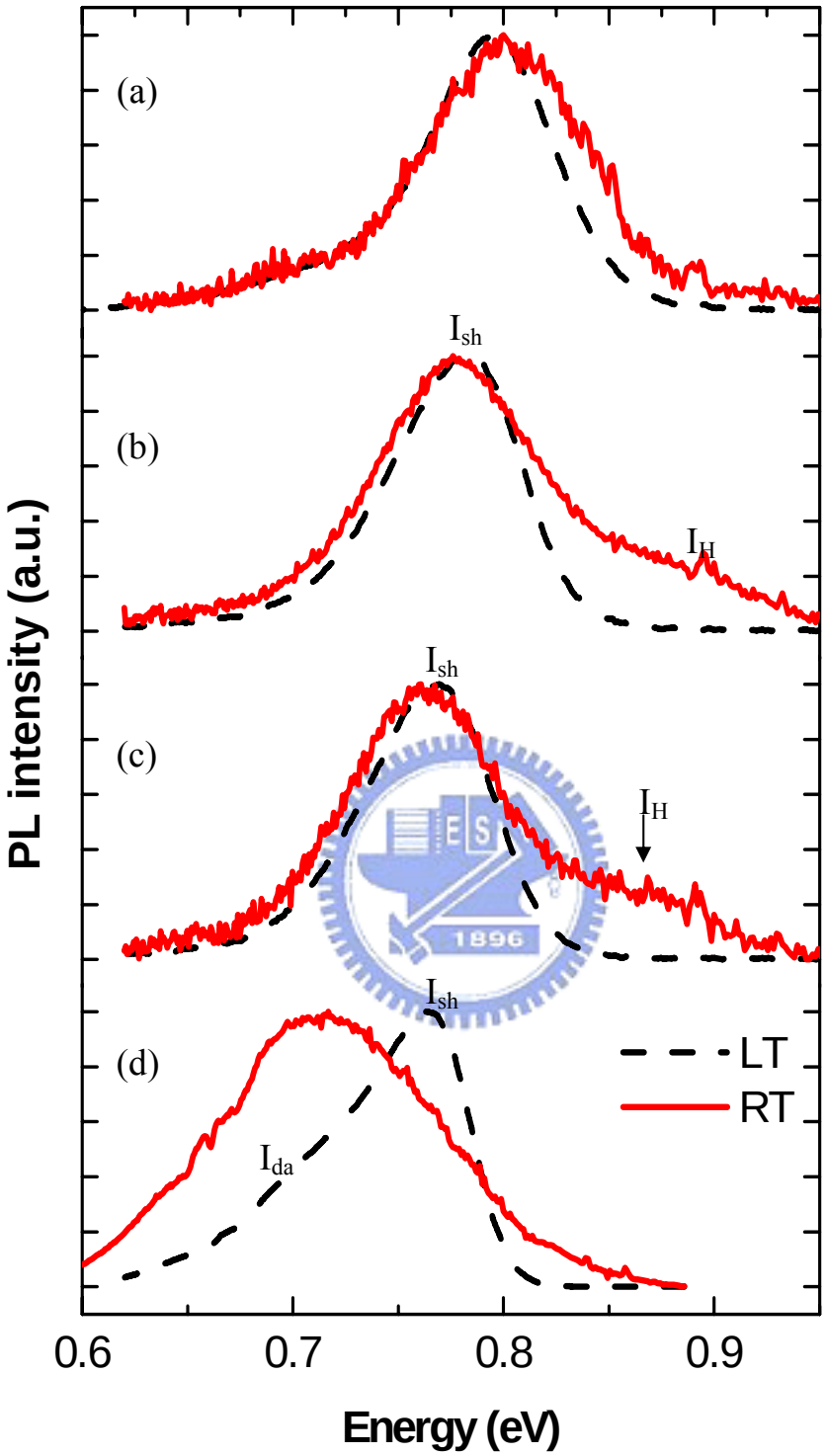

Fig. 4-12. Normalized PL spectra at 17K (dashed line) and 300K (solid line) of (a) InN 18 nm-dots, (b) InN 28 nm-dots (c) InN 32 nm-dots, and (d) the InN epilayer.

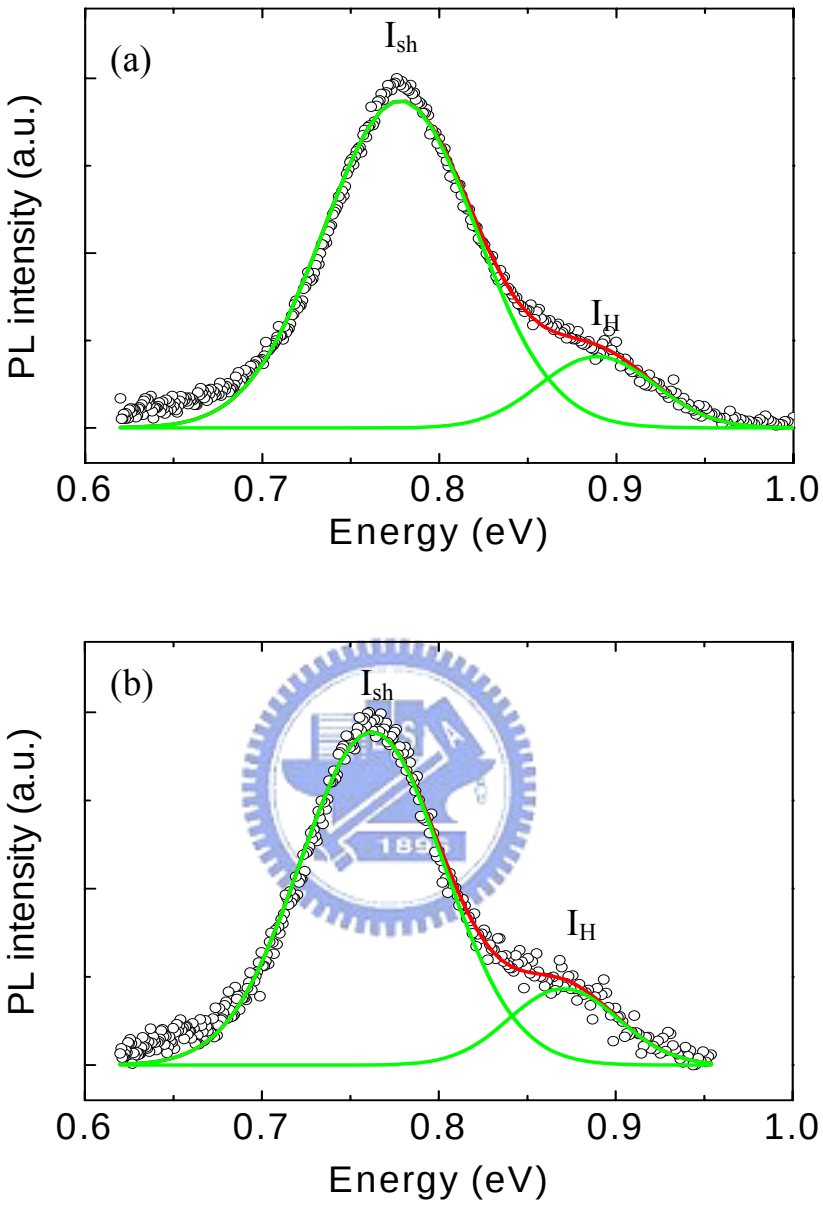

Fig. 4-13. The solid line is the Gaussian fitting curve, and the hollow circle is the PL data at 300K of (a) InN 28 nm-dot and (b) InN 32 nm-dot.

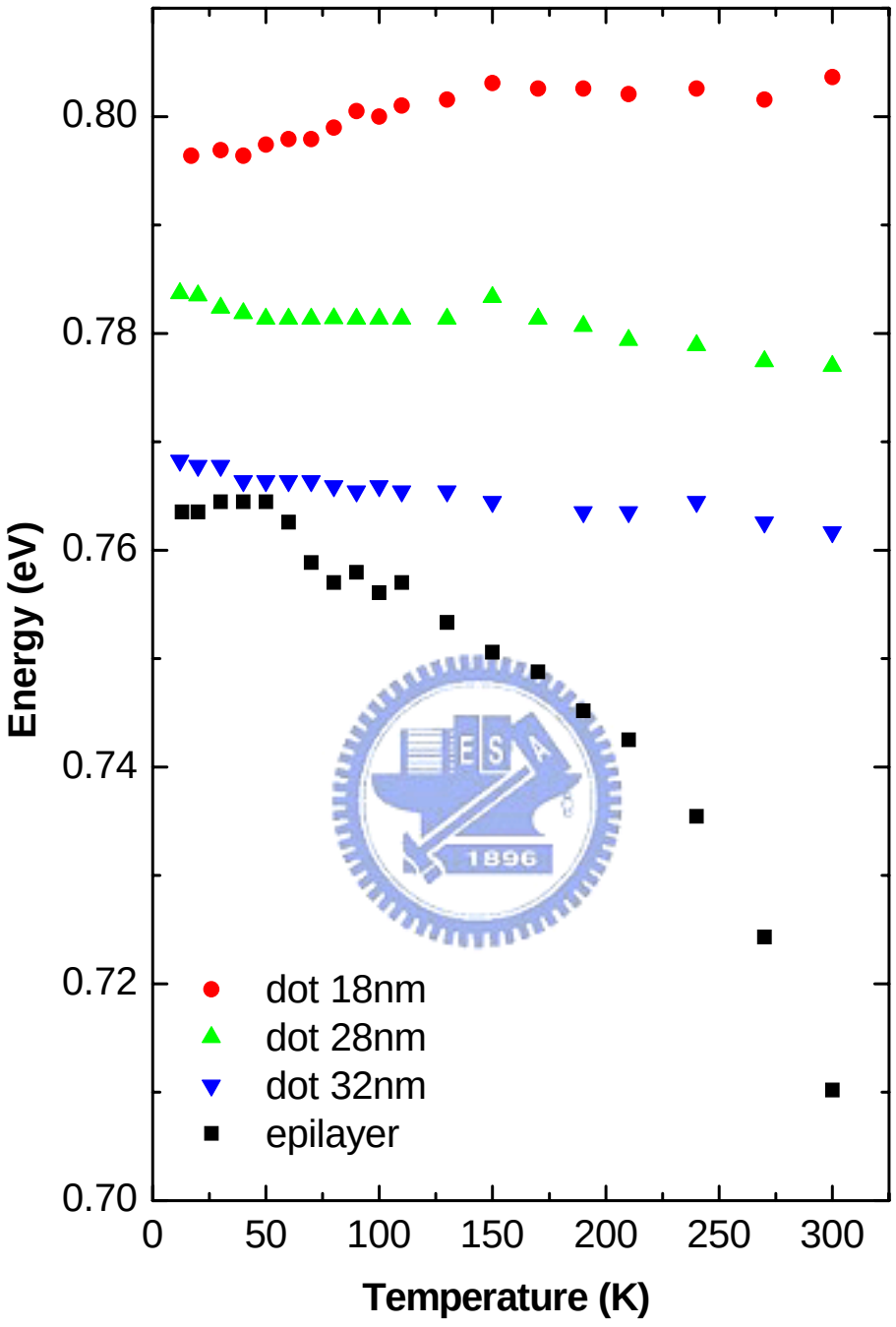

Fig. 4-14. PL peak energies as a function of temperature for the InN epilayer and dots.

4-3-2 Temperature-dependent PL integrated intensity

In order to understand the mechanism of PL quenching, the temperature dependence of the PL integrated intensity is studied, as shown in Fig. 4-15. These data can be theoretically fitted by the Arrhenius equation,

$$I(T) = \frac{I(0)}{1 + C_1 e^{-E_a / k_B T} + C_2 e^{-E_b / k_B T}},$$

where I(T) and I(0) are the individually integrated intensity at temperatures T and 0 K, C_1 and C_2 are fitting parameters, and E_a and E_b are thermal activation energies which domain at the low and high temperature region, respectively.

The activation energies (E_{a1} and E_{a2}) of the InN epilayer are about 8 meV and 61 meV at the low and high temperature range. We believe that the activation energy of E_{a1} is contributed to the binding energy of holes at shallow acceptors and the activation energy of E_{a2} is ascribed to the binding energy of holes at deep acceptors in the epilayer. The quenching mechanisms may be caused by holes thermally de-trapped from shallow and deep acceptor states into the valance band.

From the Arrhenius equation, two activation energies (E_{a1} and E_{a3}) can be obtained for InN dots. The activation energies (E_{a1}) of InN dots are about 10 meV and similar to E_{a1} of the epilayer. As a result, the activation energies (E_{a1}) of the InN dots can be assigned to the binding energy of shallow acceptors. Carriers may be thermally delocalized from shallow acceptor states into the valence band.

The activation energies (E_{a3}) of InN dots are 81±11, 90±9 and 89±15 meV. In our samples, the energy difference between InN dots and GaN barrier is about 2.6 eV, and this energy is much larger than the value of E_{a3}, so it's impossible that carriers in quantum dot states are thermally activated into the barrier state.

Moreover, the activation energies (E_{a3}) are close to the energy differences between I_H and I_{sh} for 28 nm- and 32 nm-dots at room temperature are 110 meV and 100 meV. Furthermore, as shown in Fig. 4-16, if we ignore the high-energy shoulder, I_H, and use only one peak (I_{sh}) to fit the PL integrated intensity inverse temperature plot. Two activation energies of E'_{a1}=8±1 meV and E'_{a3}=83±12 meV can be obtained by the Arrhenius fitting and are close to those considering the integrated intensity of the high-energy shoulder. Therefore, we believe that E_{a3} is the thermal activation energy for carriers from I_{sh} state to I_H state.

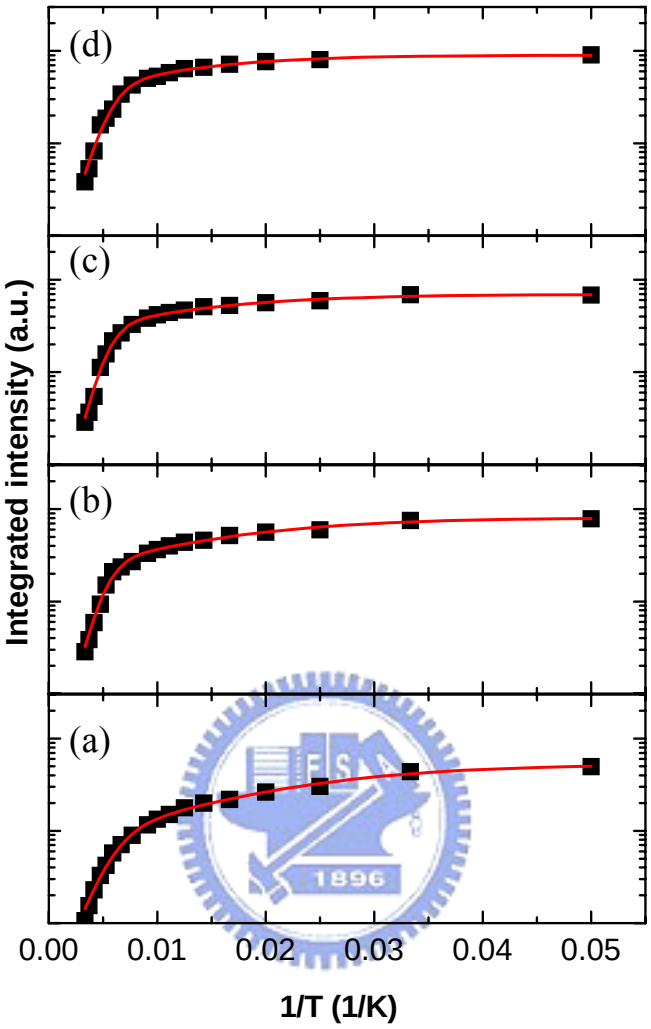

Fig. 4-15. Temperature dependence of the PL integrated intensity:
(a) the InN epilayer with E_{a1}=8±1meV and E_{a2}=61±13 meV, (b) InN 32 nm-dots with E_{a1}=9±1 meV and E_{a3}=89±15 meV, (c) InN 28 nm-dots with E_{a1}=9±1 meV and E_{a3}=90±9 meV and (d) InN 18 nm-dots with E_{a1}=10±1 meV and E_{a3}=81±11 meV.

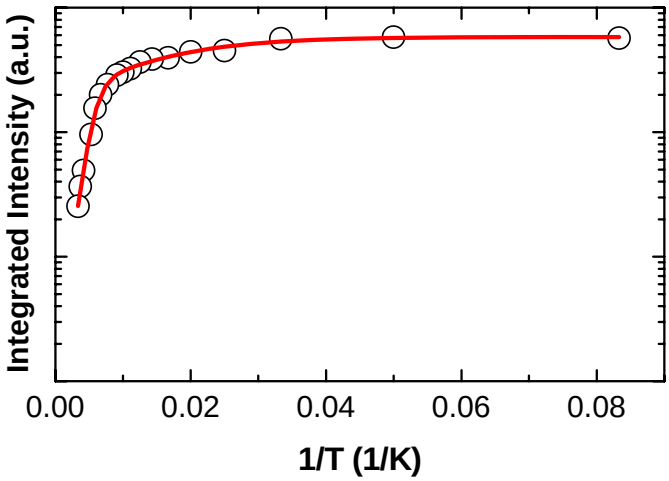

Fig. 4-16. The hollow circle is the PL integrated intensity versus inverse temperature for InN 32 nm-dot with E'_{a1}=8±1 meV and E'_{a3}=83±12 meV and the solid line is the fitting curve using Arrhenius equation.